Improved CFO Synchronization of Dual-Polarized OFDM Systems using Training Symbols

José Luis Hinostroza N., Osmar Tormena Jr, Silvio O. e Silva Jr. and Luís Geraldo P. Meloni

***Abstract*— In 5G and next-generation communications systems, as well as at wireless transmission using millimeter waves, dual polarization systems have gained recent interest. This paper presents carrier frequency offset (CFO) synchronization technique for Dual-Polarized Orthogonal Frequency Division Multiplexing (DP-OFDM) based on the transmission of training symbols. The derived techniques lead to enhancing in performance in terms of variance of estimator against classic single-polarized (SP) complex version by using the same radiated power for fair comparisons. The synchronization technique and the Cramér-Rao lower bound are derived using quaternion algebra, which prove and corroborate along with simulations to the observed improvement in performance.**

***Keywords*— OFDM CFO synchronization, quaternion OFDM, CRLB, training symbol.**

I. Introduction

Over the past decades, Orthogonal Frequency Division Multiplexing (OFDM) has been widely adopted in a number of standard physical layers at variate applications, e.g. WLAN, digital television, Internet of Things, among many others. OFDM main advantages are high spectral efficiency and immunity to frequency selective fading. However, as it has been shown at the technical literature, OFDM is highly susceptible to carrier frequency offsets (CFO); as a matter of fact, in order to keep Signal-to-Interference Ratio (SIR) lower than 20 dB, frequency offset must be below 4% of inter-carrier separation [1], [2]. The use of training sequences (TS) for frame timing and carrier frequency synchronization in OFDM was proposed by Schmidl and Cox in [3]. The following works proposed solutions to deal with a drawback caused by a plateau in the time metric of Schmidl and Cox algorithm [4] aiming to improve performance. On the other hand, dual-polarized antennas are used in 5G trials and deployments to improve spectral efficiency in massive MIMO systems using millimeter wave bands [5], [6].

In recent years, the use of hyper-complex algebras, and particularly quaternions, has paved the way for new approaches with performance gains over the classical ones for designing orthogonal space-time block codes [7], as well as for modeling both OFDM dual-polarized schemes [8] and MIMO systems with flexible combination of time, space, frequency and polarization diversities [9]. In that sense, the use of quaternion algebra in frequency synchronization techniques based on training sequences for dual-polarized OFDM schemes is explored in the present work.

The paper is organized as follows. In section II, a brief review of quaternion algebra is presented. In next section, a description of dual-polarized systems using quaternions is outlined. Section IV presents the modified algorithm for CFO estimation, which performance is demonstrated through simulations in Section V. The paper is concluded in followed section and the CRLB demonstration for the proposed algorithm is derived in Appendix I.

Luís Geraldo P. Meloni, José Luis Hinostroza N. and Silvio O. e Silva Jr. are with the School of Electrical and Computer Engineering, University of Campinas, Campinas, SP, Brazil. E-mails: meloni@decom.fee.unicamp.br, hinos.jl@decom.fee.unicamp.br and silvio@decom.fee.unicamp.br.

Osmar Tormena Jr. is with the Academic Department of Electronics, Federal University of Technology - Paraná, Campo Mourão, PR, Brazil. E-mail: tormena@utfpr.edu.br.

II. Quaternion preliminaries

Quaternion algebra, usually denoted as $\mathbb{H}$, is an hyper-complex number system conceived by William R. Hamilton in 1843 [10], in an attempt to extend division algebras to orders higher than two. Quaternion q is represented in the form:

$$q = a + b\boldsymbol{i} + c\boldsymbol{j} + d\boldsymbol{k}, \tag{1}$$

where a, b, c, $d \in \mathbb{R}$ and $\{\boldsymbol{i}, \boldsymbol{j}, \boldsymbol{k}\}$ are imaginary units which squares and products satisfy $\boldsymbol{ij} = -\boldsymbol{ji} = \boldsymbol{k}$, $\boldsymbol{jk} = -\boldsymbol{kj} = \boldsymbol{i}$, $\boldsymbol{ki} = -\boldsymbol{ik} = \boldsymbol{j}$, $\boldsymbol{i}^2 = \boldsymbol{j}^2 = \boldsymbol{k}^2 = -1$. These relationships, in turn, refer to the non-commutative multiplication operation of quaternions.

A quaternion can be decomposed into scalar and vector parts, respectively, $\mathcal{R}(q) = a$, and $\mathcal{V}(q) = b\boldsymbol{i} + c\boldsymbol{j} + d\boldsymbol{k}$. If $\mathcal{V}(q) = 0$, the quaternion q is called scalar, and if $\mathcal{R}(q) = 0$, q is denoted as pure quaternion. The imaginary parts with respect to $\boldsymbol{i}$, $\boldsymbol{j}$, and $\boldsymbol{k}$ are respectively $\mathcal{I}_i(q) = b$, $\mathcal{I}_j(q) = c$, and $\mathcal{I}_k(q) = d$. In the case of complex numbers, $\mathcal{R}_e(z)$ and $\mathcal{I}_m(z)$ denote real and imaginary parts of $z \in \mathbb{C}$, respectively.

A quaternion conjugate is defined as $q^* = a - b\boldsymbol{i} - c\boldsymbol{j} - d\boldsymbol{k}$. The norm and module are respectively $\parallel q \parallel = qq^* = q^*q$ and $|q| = \sqrt{\parallel q \parallel}$ [10]; if $\parallel q \parallel = 1$, the quaternion q is called unitary. Besides, the set of pure unitary quaternions are the points over the surface of a sphere of unit radius in the space formed by the axis $\boldsymbol{i}, \boldsymbol{j}$, and $\boldsymbol{k}$, and also the solutions to $q^2 = -1$.

Another useful representation, denominated Cayley-Dickson (CD) decomposition [10], splits a quaternion into two complex numbers lying in orthogonal Argand 2-D planes. Namely, $q = q_1 + q_2\boldsymbol{j}$, where $q_1 = a + b\boldsymbol{i}$ and $q_2 = c + d\boldsymbol{i}$, are the simplex and perplex parts of q, denoted by the operators $\mathcal{S}(q)$ and $\mathcal{P}(q)$ respectively.

III. Dual-polarized Quaternion OFDM

OFDM systems are based on Fourier transform. For quaternion algebra, several discrete Fourier transform have been

defined. Since quaternion algebra is non-commutative, the left-sided discrete quaternion Fourier transform has been used in [8], [9] for quaternion OFDM, that is

$$X_k = \sum_{n=0}^{N-1} e^{-\boldsymbol{i}2\pi kn/N}\, x_n, \tag{2}$$

where x_n is a quaternion sequence. The quaternion OFDM transceiver is illustrated in Fig. 1.

In the transmitter, at the serial-to-parallel conversion block, N samples are stored for consequential computation by the left-sided inverse discrete quaternion Fourier transform [8]

$$x_n = \frac{1}{N}\sum_{k=0}^{N-1} e^{\boldsymbol{i}2\pi kn/N}\, X_k, \quad \text{for } n = 0, ..., N-1. \tag{3}$$

In the above equation, X_k is equal to a quaternion vector Q_m for symbol m in Fig. 1, constructed by use of the Cayley-Dickson form

$$Q_m = Q_{m,1} + Q_{m,2}\boldsymbol{j}, \tag{4}$$

where $Q_{m,1}$, $Q_{m,2}$ are complex-valued in a space orthogonal to $\boldsymbol{j}$, and $Q_m \in \mathbb{H}$. This quaternion representation separates a quaternion into two Argand planes [11], perpendicular to each other, intercepting at the 4-D space origin. Incoming bit-streams are separated into two groups $b_{0,i}$ and $b_{1,i}$, for $0 \leq i \leq N_b$, each group defines an independent constellation with 4^{N_b} points, where N_b is the number of bits for defining one point in the Argand plane constellation.

Classical fast Fourier transform algorithms can be used to implement the inverse discrete quaternion Fourier transform, which is performed in the next block. However, the algorithms complexity for quaternions transforms is twice of the classical ones [11, p. 60], [12].

At transmit side, samples are prepared by performing cyclic extension processing, which copies $(M = N + N_c)$ ending samples into the beginning of the block to facilitate demodulation. It also provides subcarrier orthogonality.

After parallel-to-serial conversion, the symplectic decomposition is performed in order to enable the signals transmission by two independent antenna arrays using cross-polarized waves. The last blocks, consisting of pulse shaper, digital-to-analog conversion, mixer, and power amplifier blocks are well known in wireless communications systems.

After the analog-to-digital and down-conversion, at the receiver end of Fig. 1, the symplectic form in sequence data is realized by (4). Before direct discrete quaternion Fourier transform can be performed, data must be parallelized and the cyclic extension must be removed. Data equalization may be carried out in Fourier as well as in time domain. Complex equalizer and demodulator blocks can be used right after the quaternion equalizer block, since the symplectic decomposition is performed in the latter.

Regarding the link model of the channel, a simple model can be represented by

$$H_m^{\times} = \begin{bmatrix} h_m^{11} & h_m^{12} \\ h_m^{21} & h_m^{22} \end{bmatrix}, \tag{5}$$

where each element is a complex channel gain, h_m^{11} and h_m^{22} are signals received with the same polarization, and h_m^{12} and h_m^{21} gains for cross-polar scatter. More detailed descriptions for link model can be found in [8], [9].

IV. Synchronization based on training symbols

Synchronization based on training sequence is used in OFDM systems operating at bursty packaged data using a frame structure. The method presented in this section can be applied to find the start of the frame, as well as for CFO estimation by the use of training sequences present in one or more consecutive OFDM symbols. This technique for complex OFDM was proposed in [3], which uses a periodic training sequence known as preamble, consisting of one or two OFDM symbols transmitted at the beginning of the frame. These training symbols are constructed so that, apart from the cyclic extension, they exhibit in time domain two equal halves. For this purpose, it is possible to conceive these sequences by a pseudo-noise (PN) generator applied directly in time domain, as well as in frequency domain, where the PN sequence is transmitted at even sub-carrier frequencies, and zeros are placed at odd ones. Therefore, the inverse Fourier transform exhibits the desired symmetry in time. These training sequences are used to detect the frame start. It can also be used for refining CFO estimation, allowing fractional CFO, denoted by ϵ, where $\epsilon < 1$. The carrier frequency integer offset may be determined by using the second OFDM symbol. These training sequences have also an important role in fast channel response estimation, as it is for example in the case of IEEE 802.15.4, [13], where a Long Term Field (LTF), is used for fast equalization and synchronization.

The proposed method is based on estimation of partial auto-correlation function of received sequence y_n. For that, let $L = N/2$, and $\mathcal{I}$ is the cyclic prefix range as illustrated in Fig. 2. If the conjugate of a sample from the first half is multiplied by a sample at L samples apart, and considering that the channel response remains the same during a OFDM symbol, the effect of the channel should cancel, and the result will have phase $\pi\epsilon$.

By placing the training sequence quaternion samples X_0, $X_1, \ldots, X_{L-1}$ at even subcarriers of quaternion OFDM symbol, the transmit symbols in time domain are

$$x_n = x_{n,1} + x_{n,2}\boldsymbol{j} = \frac{1}{N}\sum_{l=0}^{L-1} e^{\boldsymbol{i}2\pi n(2l)/N} X_l \tag{6}$$

for $n = 0,\ 1,\ ...,\ N-1$.

Consider initially an estimator, which is justified in the sequence, computed for instant d sample-by-sample

$$\begin{aligned} P(d) &= \sum_{m=0}^{L-1} S\{r_{d+m} r_{d+m+L}^*\}, \\ R(d) &= \sum_{m=0}^{L-1} |r_{d+m+L}|^2, \end{aligned} \tag{7}$$

where $R(d)$ is used for normalization of $P(d)$. These equations may be computed recursively as

$$\begin{aligned} P(d+1) &= P(d) + S\{r_{d+L} r_{d+2L}^*\} - S\{r_d r_{d+L}^*\}, \\ R(d+1) &= R(d) + |r_{d+2L}|^2 - |r_{d+L}|^2. \end{aligned} \tag{8}$$

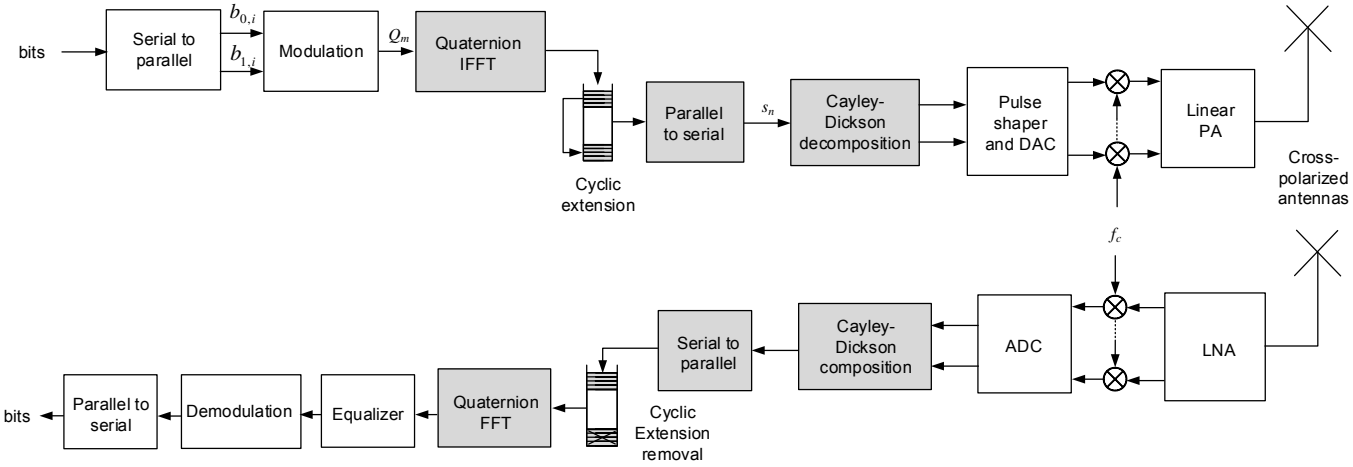

Fig. 1: Dual-polarization OFDM transceiver, the shadowed blocks are computed using quaternion algebra.

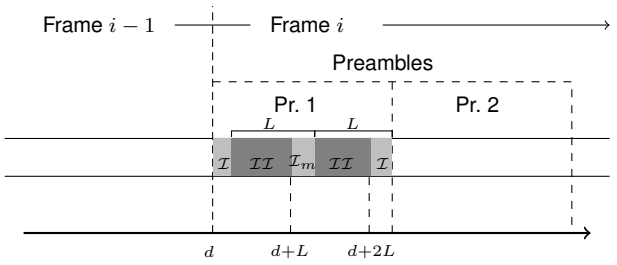

Fig. 2: Preamble sequence at frame beginning for synchronization based on training preamble, where middle samples $\mathcal{I}_m$ are identical to those of cyclic prefix $\mathcal{I}$.

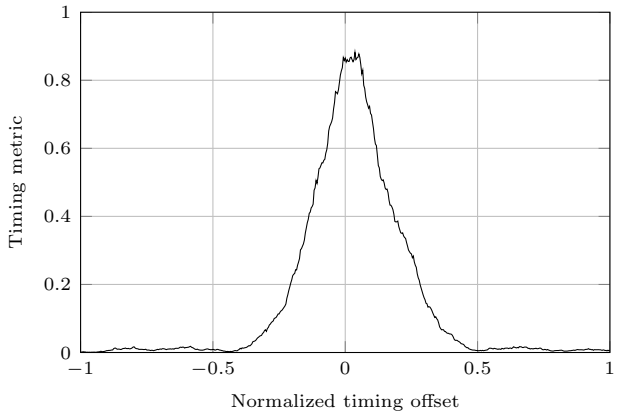

Fig. 3: Example of timing metric for synchronization based on training sequence (SNR = 10 dB).

Therefore, a time metric is defined as

$$M(d) = \frac{|P(d)|^2}{(R(d))^2}. \tag{9}$$

This metric exhibits a plateau for values of index $d \in \mathcal{I}$, and a rising and falling time equal to $N/2$ as shown in Fig. 3 for $N_c/N = 0.125$, where x-axis represents STO normalized to the OFDM symbol duration. This results are similar to the complex technique [3].

A peak detector may be used for the STO estimation. Therefore, considering the quaternion OFDM symbol already synchronized in time, the received signal for each polarization after removing the cyclic prefix are

$$r_{n,1} = y_{n,1} + z_{n,1}, \tag{10}$$

$$r_{n,2} = y_{n,2} + z_{n,2}, \tag{11}$$

where $z_{n,1}$ and $z_{n,2}$ are the AWGN components, so they are independent complex Gaussian variables with zero mean and variance $\sigma^2/2$. The signal components of $r_{n,1}$ and $r_{n,2}$ are respectively

$$\begin{aligned} y_{n,1} \quad &= \tfrac{1}{N}\textstyle\sum_{l=0}^{L-1} e^{\boldsymbol{i}2\pi n(2l+\epsilon)/N} X_{l,1} H_{2l}^{11} \\ &+ \tfrac{1}{N}\textstyle\sum_{l=0}^{L-1} e^{\boldsymbol{i}2\pi n(2l+\epsilon)/N} X_{l,2} H_{2l}^{21} \end{aligned} \tag{12}$$

and

$$\begin{aligned} y_{n,2} \quad &= \tfrac{1}{N}\textstyle\sum_{l=0}^{L-1} e^{\boldsymbol{i}2\pi n(2l+\epsilon)/N} X_{l,1} H_{2l}^{12} \\ &+ \tfrac{1}{N}\textstyle\sum_{l=0}^{L-1} e^{\boldsymbol{i}2\pi n(2l+\epsilon)/N} X_{l,2} H_{2l}^{22}. \end{aligned} \tag{13}$$

The CD compositions of these components give $r_n = r_{n,1} + r_{n,2}\boldsymbol{j}$, $z_n = z_{n,1} + z_{n,2}\boldsymbol{j}$, and $y_n = y_{n,1} + y_{n,2}\boldsymbol{j}$. Besides, we observe from (12) and (13) that

$$y_{n+L,1} = e^{\boldsymbol{i}\pi\epsilon} y_{n,1}, \tag{14}$$

$$y_{n+L,2} = e^{\boldsymbol{i}\pi\epsilon} y_{n,2}, \tag{15}$$

and therefore $y_{n+L} = e^{i\pi\epsilon}\, y_n$, for $n = 0, 1, ..., L-1$. As consequence, it follows

$$r_n r_{n+L}^* = (y_n + z_n)(e^{\boldsymbol{i}\pi\epsilon} y_n + z_{n+L})^* \tag{16}$$

$$= |y_n|^2 e^{-\boldsymbol{i}\pi\epsilon} + y_n z_{n+L}^* + z_n y_n^* e^{-\boldsymbol{i}\pi\epsilon} + z_n z_{n+L}^*. \tag{17}$$

When considering expected values in above equation, it is evident that only the first term contains information about ϵ, and additionally, that the perplex component of this term is null. Furthermore, the last three terms represent noise components for estimation and have both simplex and perplex parts different from zero. Therefore, it is possible to suppress half of noise components by taking only the simplex part of

the terms in (17), i.e the modified estimator for quaternion case results

$$\hat{\epsilon} = -\frac{1}{\pi}\angle P(\hat{d}), \tag{18}$$

where $P(d) = \sum_{n=0}^{L-1} S\{r_{d+n} r^*_{d+n+L}\}$ is evaluated at the optimum index $\hat{d}$ inside the CP interval $\mathcal{I}$, as shown in Fig. 2. As can be observed from the above equation, the CFO estimator range is the interval $(-1, 1)$ times the frequency resolution, for $P(\hat{d})$ argument in $(-\pi, \pi)$ range.

The Cramér-Rao Lower bound (CRLB) of above estimator is derived in Appendix I, which shows a gain of 3 dB of the CFO estimator variance when compared to the complex counterpart.

As a final remark, one observe that above defined metrics $P(d)$, $R(d)$, and therefore $M(d)$, can be expressed in terms of simplex and perplex parts of the observed signal, namely

$$\begin{aligned} P(d) &= \sum_{m=0}^{L-1} (r_{d+m,1} r^*_{d+m+L,1} + r_{d+m,2} r^*_{d+m+L,2}), \\ R(d) &= \sum_{m=0}^{L-1} (|r_{d+m+L,1}|^2 + |r_{d+m+L,2}|^2), \end{aligned} \tag{19}$$

using only complex algebra. Therefore, we can observe that the use of quaternion algebra has conducted to the derivation of a new improved synchronization algorithm that can be implemented by use of only complex-valued variables.

V. Simulation Results

The algorithm presented for carrier frequency offset estimation were simulated for dual-polarized quaternion OFDM and compared to single polarized complex OFDM, considering only an ideal dual-polarization link model of the channel without cross-polarization interference. For all conducted simulations, $N = 256$ was used as the size of the FFT, and cyclic prefix size was $N_c = 64$; a total of 10^5 iterations were performed for each case. For fair comparison, the power transmission used for each element of the orthogonal polarized antenna of the quaternion case is half the power transmitted over the unique antenna of the complex case, for setting the same irradiated power of complex case. A total of 10^4 frames were transmitted in each case over the same AWGN channel. All conducted simulations use quaternion OFDM as in [8].

Simulation results are shown in Fig. 4. In this case, we used only one preamble symbol for estimating the fractional part of the CFO. Results show a minimum 3 dB gain when quaternions are compared to single-polarized OFDM [3]. This performance improvement is attributed to diversity gain resulted from using dual-polarization transmissions.

VI. Conclusions

The original Schmidl-Cox algorithm was reformulated to use quaternion algebra in order to derive a CFO synchronization technique for dual-polarized OFDM schemes. Numerical simulations showed that this reformulation outperforms its single-polarized OFDM version over the entire SNR range as expected due to diversity gain, as shown in Fig. 4. Besides, the CRLB is derived in Appendix I, which corroborates to the observed simulation results.

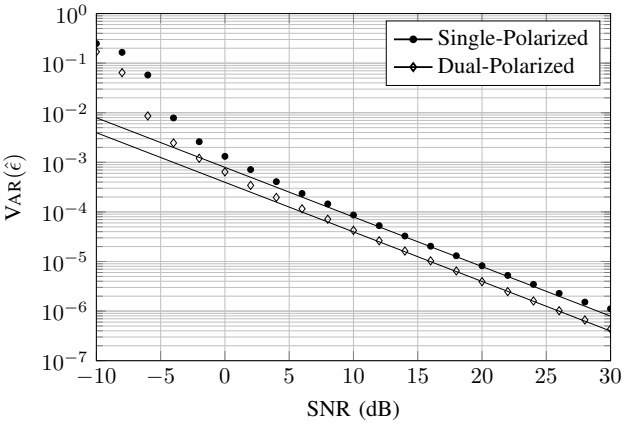

Fig. 4: CFO estimator variance compared to SP case.

Acknowledgment

This study was financed in part by the Coordenação de Aperfeiçoamento de Pessoal de Nível Superior - Brasil (CAPES) - Finance Code 001.

References

[1] T. Pollet, M. Van Bladel, and M. Moeneclaey, "Ber sensitivity of ofdm systems to carrier frequency offset and wiener phase noise," *IEEE Transactions on Communications*, vol. 43, no. 2/3/4, pp. 191–193, 1995.

[2] P. H. Moose, "A technique for orthogonal frequency division multiplexing frequency offset correction," *IEEE Transactions on Communications*, vol. 42, no. 10, pp. 2908–2914, 1994.

[3] T. M. Schmidl and D. C. Cox, "Robust frequency and timing synchronization for OFDM," *IEEE Transactions on Communications*, vol. 45, pp. 1613–1621, Dec 1997.

[4] H. Minn, V. K. Bhargava, and K. B. Letaief, "A robust timing and frequency synchronization for ofdm systems," *IEEE Transactions on Wireless Communications*, vol. 2, no. 4, pp. 822–839, 2003.

[5] S. Won, M. Mueck, V. Frascolla, J. Kim, G. Destino, A. Pärssinen, M. Latva-aho, A. Korvala, A. Clemente, T. Kim, I. Kim, H. Chung, and E. Strinati, "Development of 5G CHAMPION testbeds for 5G services at the 2018 Winter Olympic Games," in *2017 IEEE 18th International Workshop on Signal Processing Advances in Wireless Communications (SPAWC)*, pp. 1–5, Jul 2017.

[6] M. Shafi, A. F. Molisch, P. J. Smith, T. Haustein, P. Zhu, P. De Silva, F. Tufvesson, A. Benjebbour, and G. Wunder, "5g: A tutorial overview of standards, trials, challenges, deployment, and practice," *IEEE Journal on Selected Areas in Communications*, vol. 35, no. 6, pp. 1201–1221, 2017.

[7] J. Seberry, K. Finlayson, S. S. Adams, T. A. Wysocki, T. Xia, and B. J. Wysocki, "The theory of quaternion orthogonal designs," *IEEE Transactions on Signal Processing*, vol. 56, no. 1, pp. 256–265, 2008.

[8] L. G. P. Meloni, "Hypercomplex OFDM Schemes for Cross-Polarized Antennas," *2012 International Symposium on Communications and Information Technologies*, vol. 1, no. 1, pp. 1–6, 2012.

[9] L. Meloni, J. H. N., and O. T. Jr., "Construction and Analysis of Quaternion MIMO-OFDM Communications Systems," *Journal of Communication and Information Systems*, vol. 32, pp. 80–89, Jan 2017.

[10] T. A. Ell, N. Le Bihan, and S. J. Sangwine, *Quaternion Fourier Transforms for Signal and Image Processing*. Wiley-IEEE Press, 1st ed., 2014.

[11] T. Ell and S. Sangwine, "Hypercomplex Fourier transform of colour images," *IEEE Trans. Image Process.*, vol. 16, pp. 22–35, Jan 2007.

[12] S. Said, N. L. Bihan, and S. Sangwine, "Fast complexified quaternion Fourier transform," *IEEE Trans. on Signal Processing*, vol. 56, no. 4, pp. 1522–1531, 2008.

[13] "IEEE Standard for Low-Rate Wireless Networks," *IEEE Std 802.15.4-2015 (Rev. IEEE Std 802.15.4-2011)*, pp. 1–709, 2016.

APPENDIX I
CRLB FOR CFO ESTIMATION

In [3], authors showed that a CFO estimator obtained by partial correlation in time domain, as the one derived in (18), is the maximum-likelihood estimator (MLE), and consequently attains the Cramér-Rao Lower Bound (CRLB) at high SNR. Thus, appealing to the isomorphism between complex and quaternion estimators, one can conclude that proposed estimator also attains its respective CRLB under the same condition. In order to obtain the variance of the proposed estimator, the method in [2] is used. It should be noted that $P(\hat{d}) \in \mathbb{C}_i$ is a complex number with angle $-\pi\hat{\epsilon}$, so the rotated complex $P(\hat{d})e^{i\pi\epsilon}$ has $\arg(P(\hat{d})e^{i\pi\epsilon}) = -\pi\hat{\epsilon} + \pi\epsilon = -\pi(\hat{\epsilon} - \epsilon)$, from which the estimation error is derived as

$$\hat{\epsilon} - \epsilon = -\frac{1}{\pi}\arg[\sum_{n=0}^{L-1} S\{r_{\hat{d}+n} r^*_{\hat{d}+n+L}\}e^{i\pi\epsilon}]. \tag{20}$$

As we are interested in the variance of CFO estimation, given that time synchronization was previously carried out, we can consider $\hat{d} = 0$, without loss of generality. Besides, as complex factor $e^{i\pi\epsilon} \in \mathbb{C}_i$, it can be placed inside the simplex operator. Therefore

$$\hat{\epsilon} - \epsilon = -\frac{1}{\pi}\arctan\left(\frac{\mathcal{I}_m[\sum_{n=0}^{L-1} S\{r_n r^*_{n+L}e^{i\pi\epsilon}\}]}{\mathcal{R}_e[\sum_{n=0}^{L-1} S\{r_n r^*_{n+L}e^{i\pi\epsilon}\}]}\right) \tag{21}$$

$$= -\frac{1}{\pi}\arctan\left(\frac{\sum_{n=0}^{L-1}\mathcal{I}_i[r_n r^*_{n+L}e^{i\pi\epsilon}]}{\sum_{n=0}^{L-1}\mathcal{R}[r_n r^*_{n+L}e^{i\pi\epsilon}]}\right), \tag{22}$$

which, for SNR high enough to produce small estimation errors, reduces to

$$\hat{\epsilon} - \epsilon \approx -\frac{1}{\pi}\frac{\sum_{n=0}^{L-1}\mathcal{I}_i[r_n r^*_{n+L}e^{i\pi\epsilon}]}{\sum_{n=0}^{L-1}\mathcal{R}[r_n r^*_{n+L}e^{i\pi\epsilon}]}. \tag{23}$$

Besides, by repeating (17) for convenience,

$$r_n r^*_{n+L}e^{i\pi\epsilon} = |y_n|^2 + y_n z^*_{n+L}e^{i\pi\epsilon} + z_n y^*_n + z_n z^*_{n+L}e^{i\pi\epsilon}, \tag{24}$$

leads up to $E[r_n r^*_{n+L}e^{i\pi\epsilon}] = |y_n|^2$, due to independence between signal and noise, and to the fact of z_n is WGN.

In (24), it should be noted that last term corresponds to a product of two i.i.d quaternion Gaussian r.v's, namely z_n and $z^*_{n+L}e^{i\pi\epsilon}$. At high SNR, the p.d.f of this term becomes more concentrated around the origin of 4D-space than its individual factors, which appear in second and third terms weighted by deterministic signal samples y_n and y^*_n respectively. In other words, at high SNR, last term is distributed over a 4-D sphere of ratio much lower than for the second and third terms. Thus, in the sake of simplicity, we can henceforth ignore the last term. Also, notice that first term in the right side of (24) is deterministic since expected values are taken with respect to noise components, so let

$$\alpha_n = y_n z^*_{n+L}e^{i\pi\epsilon} + z_n y^*_n, \tag{25}$$

the random part of $r_n r^*_{n+L}e^{i\pi\epsilon}$ in (24). Under the assumption that both z_n and z_{n+L} are circularly symmetric and independent, it follows that α_n is also circularly symmetric, i.e. its real and three imaginary parts are zero-mean i.i.d Gaussian real r.v's. Thus, numerator and denominator at right side of (23) are independent, so that expected value can be distributed, then it follows that $E[\hat{\epsilon} - \epsilon] \approx 0$, i.e. the estimator is unbiased, and $\text{VAR}[\hat{\epsilon}] = E[(\hat{\epsilon} - \epsilon)^2]$ reduces to

$$\text{VAR}[\hat{\epsilon}] = \frac{1}{\pi^2}\frac{E\left[\left(\sum_{n=0}^{L-1}\mathcal{I}_i[\alpha_n]\right)^2\right]}{E\left[\left(\sum_{n=0}^{L-1}(|y_n|^2 + \mathcal{R}[\alpha_n])\right)^2\right]}. \tag{26}$$

As aforementioned, real and imaginary parts of α_n are zero mean Gaussian real r.v's, each one with variance equal to a quarter of $\text{VAR}[\alpha_n]$, i.e

$$\text{VAR}[\mathcal{R}[\alpha_n]] = \text{VAR}[\mathcal{I}_i[\alpha_n]] = \frac{1}{4}E\Big[|\alpha_n|^2\Big] \tag{27}$$

$$= \frac{1}{4}E\Big[|y_n|^2|z_{n+L}|^2 + |z_n|^2|y_n|^2 + y_n z^*_{n+L}e^{i\pi\epsilon}y_n z^*_n + z_n y^*_n e^{-i\pi\epsilon}z_{n+L}y^*_n\Big] \tag{28}$$

$$= \frac{1}{4}|y_n|^2\Big(E[|z_{n+L}|^2] + E[|z_n|^2]\Big) = \frac{\sigma^2}{2}|y_n|^2. \tag{29}$$

This result, along with the independence between α_n and α_m, for $n \neq m$, implies that

$$\sum_{n=0}^{L-1}\mathcal{I}_i[\alpha_n] \sim N(0, \frac{\sigma^2}{2}\sum_{n=0}^{L-1}|y_n|^2) \tag{30}$$

$$\sum_{n=0}^{L-1}(|y_n|^2 + \mathcal{R}[\alpha_n]) \sim N(\sum_{n=0}^{L-1}|y_n|^2, \frac{\sigma^2}{2}\sum_{n=0}^{L-1}|y_n|^2). \tag{31}$$

Therefore, (26) reduces to

$$\text{VAR}[\hat{\epsilon}] = \frac{1}{\pi^2}\frac{\frac{\sigma^2}{2}\sum_{n=0}^{L-1}|y_n|^2}{\frac{\sigma^2}{2}\sum_{n=0}^{L-1}|y_n|^2 + \left(\sum_{n=0}^{L-1}|y_n|^2\right)^2} \tag{32}$$

$$= \left[\pi^2\Big(1 + \frac{\sum_{n=0}^{L-1}|y_n|^2}{\sigma^2/2}\Big)\right]^{-1}. \tag{33}$$

In above equation, for L high enough, an approximation of the sum of the numerator is $L\sigma_y^2$, where σ_y^2 is the mean power of the signal. Using this result, (33) expressed in terms of $\text{SNR} = \sigma_y^2/\sigma^2$ gives

$$\text{VAR}[\hat{\epsilon}] = \frac{1}{\pi^2(1 + 2L\ \text{SNR})}, \tag{34}$$

which, for high SNR, gives the bound

$$\text{CRLB} = \frac{1}{2\pi^2 L\ \text{SNR}}. \tag{35}$$